Energy Conversion and Management 106 (2015) 322–336

Contents lists available at ScienceDirect

Energy Conversion and Management

journal homepage: www.elsevier.com/locate/enconman

Performance and emissions of a dual-fuel pilot diesel ignition engine operating on various premixed fuels

Amin Yousefi [a,b,*], Madjid Birouk [b], Benjamin Lawler [c], Ayatallah Gharehghani [a]

[a] Department of Mechanical Engineering, Amirkabir University of Technology, Tehran, Iran
[b] Department of Mechanical Engineering, University of Manitoba, Winnipeg, Manitoba R3T 5V6, Canada
[c] Department of Mechanical Engineering, Stony Brook University, Stony Brook, NY 11794, USA

ARTICLE INFO

Article history:
Received 24 May 2015
Accepted 12 September 2015
Available online 2 October 2015

Keywords:
Dual-fuel engine
Premixed fuel types
Natural gas
Methanol
Hydrogen

ABSTRACT

A multi-dimensional computational fluid dynamics (CFD) model coupled with chemical kinetics mechanisms was applied to investigate the effect of various premixed fuels and equivalence ratios on the combustion, performance, and emissions characteristics of a dual-fuel indirect injection (IDI) pilot diesel ignition engine. The diesel fuel is supplied via indirect injection into the cylinder prior to the end of the compression stroke. Various premixed fuels were inducted into the engine through the intake manifold. The results showed that the dual-fuel case using hydrogen/diesel has a steeper pressure rise rate, higher peak heat release rate (PHRR), more advanced ignition timing, and shorter ignition delay compared to the natural gas/diesel and methanol/diesel dual-fuel cases. For leaner mixtures ($\Phi_P < 0.32$), the hydrogen/diesel case has a higher indicated mean effective pressure (IMEP) and indicated thermal efficiency (ITE); however, the methanol/diesel case has the maximum IMEP and ITE for richer mixtures ($\Phi_P > 0.32$). For instance, with an equivalence ratio of 0.35, the ITE is 56.24% and 60.85% for hydrogen/diesel and methanol/diesel dual-fuel cases, respectively. For an equivalence ratio of 0.15, the natural gas/diesel simulation exhibits partial burn combustion and thus results in a negative IMEP. At equivalence ratios of 0.15, 0.2, and 0.25, the methanol/diesel case experiences misfiring phenomenon which consequently deteriorates the engine performance considerably. As for the engine-out emissions, the hydrogen/diesel results display carbon monoxide (CO) free combustion relative to natural gas/diesel and methanol/diesel engines; however, considerable amount of nitrogen oxides (NO_x) emissions are produced at an equivalence ratio of 0.35 which exceeds the Euro 6 NO_x limit. Due to the larger area exposed to high temperature regions and the higher content of oxygen with increased methanol, soot and CO emissions are significantly reduced for richer premixed methanol mixtures. According to these findings, a dual-fuel engine operating on methanol and diesel performs better at rich conditions, whereas the performance of hydrogen and diesel is superior to that of natural gas/diesel and methanol/diesel mixtures at lean conditions.

1. Introduction

The ever increasing fossil fuel price and stringent emission regulations have led researchers to put more focus on the high efficiency and low emissions combustion concepts as well as alternative fuels for internal combustion (IC) engine applications. Particulate matter (PM) and NO_x are the main detrimental pollutant emissions generated by diesel engines. Several concepts have been investigated to reduce these emissions such as low temperature combustion (LTC), as well as using alternative fuels [1,2]. One of the emerging LTC concepts for the compression ignition (CI) mode is the homogeneous charge compression ignition (HCCI) combustion which enables achieving high thermal efficiency and ultra-low NO_x and soot emissions. However, this technology still suffers from the inability to control auto-ignition which is the major obstacle for the implementation of HCCI combustion in practical engines [3–5]. In order to address this issue, many research efforts and development endeavors have been focused on dual-fuel pilot diesel ignition engine concept, where the premixed fuel is ignited by a small amount of diesel fuel [6,7]. On the other hand, the demand for alternative/renewable fuels is increasing dramatically in the transportation sector as well as other industrial applications in order to meet the stringent emissions regulations and to reduce the dependency on conventional fossil fuels [8].

* Corresponding author at: Department of Mechanical Engineering, University of Manitoba, Winnipeg, Manitoba, Canada. Tel.: +1 204 293 6164.
E-mail addresses: yousefia@myumanitoba.ca, amin_50@yahoo.com (A. Yousefi).

http://dx.doi.org/10.1016/j.enconman.2015.09.056
0196-8904/

Nomenclature

ABDC	after bottom dead center
ATDC	after top dead center
AFR	air fuel ratio
BDC	bottom dead center
BBDC	before bottom dead center
BSFC	break specific fuel consumption
BTE	break thermal efficiency
BTDC	before bottom dead center
CI	compression ignition
CO	carbon monoxide
CO_2	carbon dioxide
CAD	crank angle degree
CA_{10}	crank angle for 10% burnt fuel
CFD	computational fluid dynamic
CN	cetane number
EVC	exhaust valve close
EVO	exhaust valve open
HRR	heat release rate
HCCI	homogeneous charge compression ignition
IC	internal combustion
IDI	indirect injection
IMEP	indicated mean effective pressure
ISFC	indicated specific fuel consumption
ITE	indicated thermal efficiency
IVC	inlet valve close
IVO	inlet valve open
LTC	low temperature combustion
NO_x	nitrogen oxide
PFI	port fuel injected
PHHR	peak heat release rate
PM	particulate matter
rpm	revolution per minute
SI	spark ignition
SOI	start of injection
SOC	start of combustion
TDC	top dead center
THC	total hydrocarbon
UHC	unburned hydrocarbon

Therefore, a considerable amount of research is directed toward the optimization of diesel engines with the incorporation of alternative fuels. Among alternative fuels, natural gas [9,10], methanol [11,12], and hydrogen [13] are the most investigated for dual-fuel pilot diesel ignition engines.

Natural gas is the lowest-cost transportation fuel available today and has been widely used with diesel fuel in CI engines. The use of natural gas offers a lot of environmental benefits because it produces fewer emissions than conventional fossil fuels. Low carbon content and clean burn features, especially low soot/smoke, have helped the proliferation of natural gas as an alternative fuel with introduction of ever more severe emissions standards. Increased natural gas energy substitution has been found to be very effective in reducing NO_x and PM emissions while maintaining acceptable engine performance [14,15].

Methanol is an advantageous choice for diesel vehicles due to its efficient combustion, environmental benefits, low cost compared to other fuels, and its availability worldwide [16]. Emissions of unburned hydrocarbons (UHC) and CO are much lower when consuming methanol. Furthermore, methanol has a much higher latent heat of vaporization which decreases temperature considerably and consequently restricts NO_x formation. Methanol has no carbon–carbon bonds which inhibits soot formation [17,18].

Hydrogen has long been recognized as a carbon-free fuel and has several advantages when used to fuel IC engines due to its none-toxic and renewability nature, high calorific value, and environmental benefits [19]. A hydrogen-operated engine produces water vapor as its main combustion products. Moreover, hydrogen has a wide flammability range in comparison with all other fuels. As a result, hydrogen can be combusted in an IC engine over a wide range of fuel–air mixtures especially very lean mixtures where lower combustion temperature and hence NO_x emissions can be achieved [21]. However, hydrogen is not ignitable via compression in modern diesel engines as it requires an ignition source. Therefore, the auto-ignition of the diesel spray can act as a pilot to ignite the premixed mixture of hydrogen/air [21].

1.1. Literature review

Compared to diesel fuel, natural gas, methanol, and hydrogen are considered alternative fuels due to their renewable nature and abundant sources. The properties of these fuels are given in Table 1 [20,21]. Despite the various advantages of these alternative fuels, the auto-ignition is still their weakest property due to their very low cetane number (CN) in comparison with diesel fuel, especially at cold starts and light load conditions. In order to address this issue a dual-fuel pilot diesel ignition engine can be used where the main fuel fumigated into the intake air steam is ignited by a small amount of diesel fuel. Lounici et al. [22] examined the effect of dual-fuel operation on the combustion characteristics, engine performance, and emissions of a diesel engine using natural gas as the premixed fuel ignited by diesel as a pilot fuel. Their results showed that at low engine loads, the total break specific fuel consumption (BSFC) for dual-fuel mode was higher than that of the conventional diesel. However, at high and moderate loads, the total BSFC was found lower for all the examined engine speeds. Moreover, the use of natural gas for dual-fuel mode showed a reduction of soot and NO_x over a wide engine operating conditions.

Table 1
Properties of natural gas, methanol, hydrogen and diesel fuels [20,21].

	Natural gas (methane)	Methanol	Hydrogen	Diesel
Formula	CH_4	CH_3OH	H_2	$C_{12}H_{26}$–$C_{14}H_{30}$
Molecular weight (g/mol)	16	32	2	170–198
Density (g/cm^3 at 20 °C)	0.65	790	8.37E−2	820–860
Boiling temperature (°C)	−161.5	64.7	−252.9	190–280
Flash point (°C)	–	11	–	52
Auto-ignition temperature (°C)	540	470	585	300–340
Stoichiometric fuel–air ratio	0.058	0.154	0.029	0.069
Cetane number	–	3–5	–	40–55
Lower heating value (MJ/kg)	50.02	20.27	119.93	42.74

However, the total hydrocarbon (THC) emissions were found to be significantly higher for dual-fuel mode. CO emissions were also found to be higher at low and moderate loads for dual-fuel mode.

Song et al. [23] examined the application of methanol as the primary fuel in a single cylinder direct injection diesel engine. They found that the full-load power of dual-fuel operation can reach or even exceed that of the original diesel engine when a suitable minimum pilot diesel quantity is used. The equivalent BSFC was improved under high load operating conditions and dual-fuel operation showed a better fuel economy at high rates of methanol addition. Furthermore, they reported that soot emissions were reduced significantly, while only a modest reduction in NO_x emissions was observed. On the other hand, they stated that adding methanol for dual-fuel operation led to increased CO and UHC emissions.

The investigation of diesel–methanol dual-fuel combustion mode in a four-cylinder, direct-injected diesel engine was conducted by Zhang et al. [24]. Methanol was injected into the intake port to form lean air–fuel mixture which was then ignited by diesel fuel in the cylinder. They reported that, at low engine loads, the brake thermal efficiency (BTE) decreased with an increase in port-fuel-injected (PFI) methanol; however, at high engine loads, the BTE was found to be insignificantly affected by PFI methanol. The PFI methanol showed a significant increase in UHC and CO emissions, and a decrease in NO_x.

Sandalci and Karaggoz [25] investigated the combustion characteristics, emissions, and performance of hydrogen PFI in a single-cylinder, naturally aspirated diesel engine. Their results revealed that, with increasing hydrogen energy fraction, the ITE of the engine decreased and the indicated specific fuel consumption (ISFC) increased. They reported that, with an increase in hydrogen flow rate, the peak in-cylinder pressure and PHRR increased while CO, carbon dioxide (CO_2), and smoke emissions decreased. However, a dramatic increase in NO_x emissions was observed.

The impact of varying hydrogen–diesel fuel mixture proportions on engine performance and emissions of a naturally aspirated direct injection diesel engine was conducted by Talibi et al. [21]. They reported a decrease in particulates, CO, and THC emissions with a slight increase in CO_2 emissions with the addition of hydrogen at fixed diesel fuel injection period. Additionally, an increased duration of the ignition delay was observed at intermediate engine loads with hydrogen addition, which was attributed to a decreased O_2 concentration in the intake charge. This reduction of O_2 concentration leads to a reduction in a rate of low temperature reactions and delays auto-ignition.

1.2. Main objectives

According to the briefly reviewed literature mentioned above, several studies focused on the effect of the premixed air–fuel ratio and pilot diesel quantity and injection timing on the performance of a dual-fuel engine. However, the effect of premixed fuel types on engine performance and combustion characteristics in a dual-fuel pilot diesel ignition engine is still lacking. In addition, no published data can be found on the effect of IDI pilot diesel on the combustion characteristics and emissions of a dual-fuel operation. Thus, the primary objective of the present work is to examine the effect of premixed fuel types and their equivalence ratio on combustion characteristics, performance, and emissions of a diesel engine fuelled by natural gas/diesel, methanol/diesel, or hydrogen/diesel in dual-fuel IDI pilot diesel operation. To achieve the goals of this study, a 3D CFD-chemistry model has been developed to describe more accurately the complicated dual-fuel pilot diesel combustion process and emissions. The simulation results concern the in-cylinder pressure, HRR, in-cylinder peak pressure and its position, ignition delay, in-cylinder temperature contours, IMEP, ITE, and emissions of the aforementioned different premixed fuels.

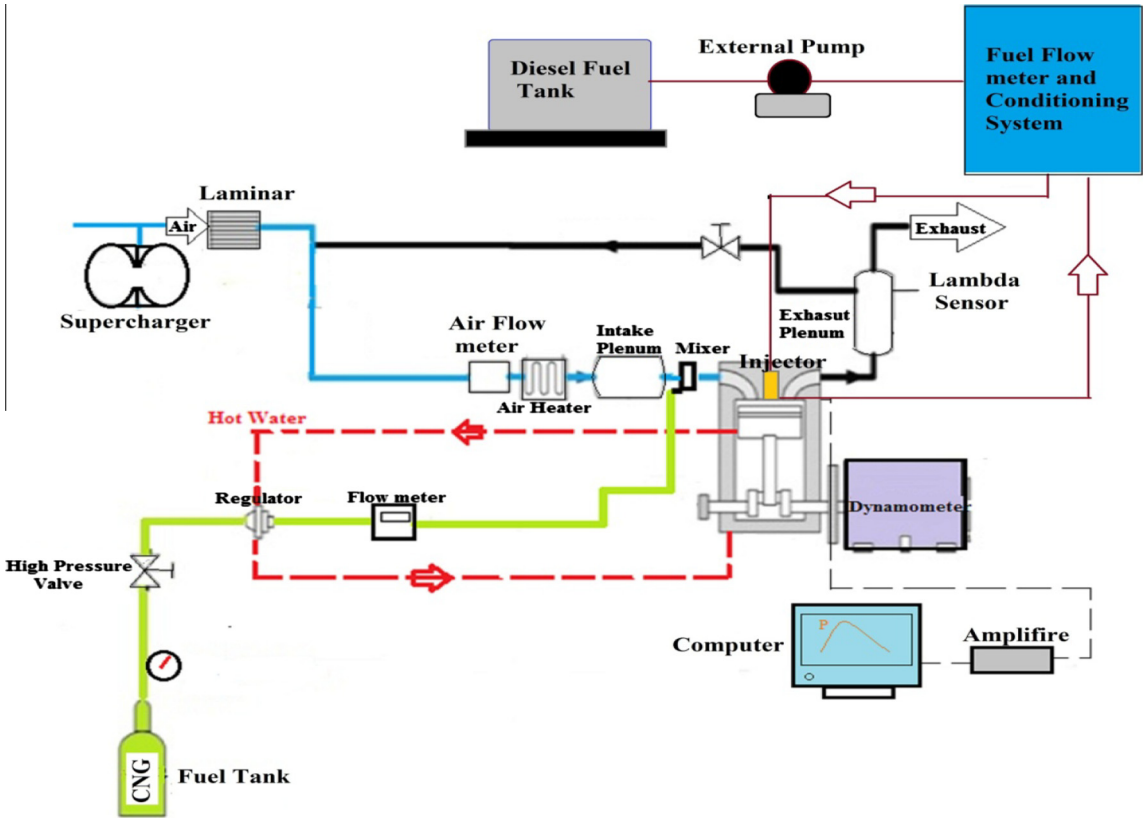

Fig. 1. Schematic of the experimental setup.

The model predictions were validated against experimental data obtained from a conventional IDI, single cylinder, supercharged Ricardo E6/MS diesel engine [26], which was modified accordingly to operate in dual-fuel (diesel and natural gas) mode where diesel fuel was used as a pilot injected fuel to ignite the premixed air–natural gas mixture. However, to ensure that the model predicts with reasonable accuracy the combustion process of hydrogen/diesel and methanol/diesel cases, model predictions were compared with published experimental data of methanol/diesel and hydrogen/diesel dual-fuel engine [20,27]. Thus, the comprehensive, validated 3D CFD-chemistry model was confidently used in the present work where a comparative assessment is carried out to investigate the impact of premixed fuel types and their equivalence ratios on engine performance and emitted pollutants.

2. Experimental setup for natural gas/diesel

Experimental data of natural gas/diesel dual-fuel combustion was obtained from a modified single-cylinder Ricardo E6/MS IDI diesel engine coupled to a DC motoring dynamometer. As shown in Fig. 2, a cylinder head with a Ricardo Comet MK.V compression swirl combustion chamber was fitted to this engine. This type of combustion chamber was made up of two parts: (1) a swirl prechamber and (2) a main combustion chamber. The swirl chamber in the head has a spherical form and the lower half is a truncated cone connected with the cylinder via a narrow throat. The main combustion chamber has cavities cut into the crown of the piston [26]. The CI engine was modified to achieve dual-fuel operation where the primary gaseous fuel (natural gas) was introduced in the intake manifold and the homogeneous air–fuel mixture was ignited by a small quantity of diesel fuel injected toward the end of the compression stroke. The diesel fuel ignites in the same way as in CI engines, and the gaseous fuel is consumed by flame propagation in a similar manner to spark ignition (SI) engines [20]. The experimental setup is shown in Fig. 1. The engine was maintained at two constant speeds of 500 and 800 rpm and run with an open throttle. The intake system encompasses a 1 kW heater incorporated within an Alcock viscous air flow meter casing. The intake air–fuel temperature was set at 380 K which was measured before the intake valve by a K-type thermocouple. Natural gas was drawn from a high-pressure cylinder and passed through a YAMATAKE flow meter to measure the flow rate of natural gas. The measured natural gas flow rate was then introduced to an intake manifold by a mixer located upstream of the intake valve to ease proper mixing. The injection of pilot diesel fuel was accomplished by a CAV injector body (type BKB 35s5153 RM) and controlled to a pressure of 150 MPa. The injection duration of the pilot diesel was set to 4 °CA. The engine out air fuel ratio (AFR) value was measured using a Lambda sensor (Bosch Isu) installed in the exhaust manifold. A 1 kW electrical heater was installed on the crankcase in order to warm up the oil before the engine start up. The oil temperature was maintained at 330 K. The temperature of the cooling water was set to 353 K. A Fotek rotary encoder with a resolution of 0.1 crank angle degree (CAD) was mounted on the engine crankshaft to monitor engine rotational speed and coordinate the pressure trace with respect to crank position. Combustion pressure was measured with a piezo-electric AVL pressure transducer (Qc43d) connected to an amplifier. An in-house computer code was developed to analyze the experimental data. The basic engine specifications, engine operating test conditions and experimental setup uncertainty for current study are listed in Tables 2–4.

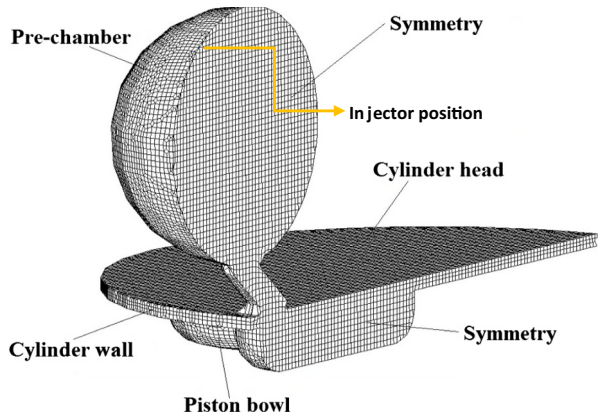

Fig. 2. Computational mesh and wall boundary conditions of Ricardo combustion chamber at TDC.

3. Numerical model and validation

3.1. 3D-CFD modeling tool

A multi-dimensional CFD model coupled with chemical kinetics (AVL FIRE-CHEMKIN) was developed in the present study which accounts for the effect of fluid flow, spray dynamics, and fuel oxidation. The governing equations included the three basic laws of conservation, continuity, and turbulence model equations. Several sub-models which were used in this study are listed in Table 5. The turbulent flow within the combustion chamber was simulated using the RNG κ–ε turbulence model [28]. Furthermore, the KH–RT (Kelvin–Helmholtz and Rayleigh–Taylor) spray break-up model was employed for the primary and secondary atomization of droplets [29]. The KH model is based on the wave model and used to predict the initial break-up of the injected blobs or the intact liquid core. The RT model was used in conjunction with the KH model to describe the secondary break-up of droplets [30]. The Dukowicz model was used for modeling heat-up and evaporation of droplets [31]. In this model, droplets were supposed to evaporate in a non-condensable gas consisting of two-component system in the gas phase (vapor and the non-condensable gas). AVL-FIRE has standard wall function for wall heat flux which accounts for the variations of gas density and turbulent Prandtl number in the boundary layer. Details of the model can be found in the Ref. [32]. As for premixed fuel oxidation, an external chemical mechanism was implemented in the CFD code to account for chemical kinetics of premixed fuel during engine cycle. The CFD code solves the average transport equations of total mixture mass, momentum and enthalpy. The CFD code feeds the species to

Table 2
Ricardo engine specifications.

Parameter	Specification
Engine type	Single cylinder E6/MS
Bore (mm)	76.2
Stroke (mm)	110
Displacement (cc)	501
Compression ratio	17.2:1
Injection type	IDI
Injection duration (°CA)	4
Nozzle hole × diameter (mm)	1 × 0.6
IVC (°ABDC)	36
IVO (°BTDC)	7
EVC (°ATDC)	7
EVO (°BBDC)	36

Table 3
Operating/test conditions for two different engine test cases.

Simulation case	Case 1	Case 2
Pressure at IVC (bar)	1.3	1.4
Intake temperature (K)	340	340
Engine speed (rpm)	500	800
Diesel fuel flow rate (mg/cycle)	2.38	1.625
Injection timing (°BTDC)	2	2
Φ_P (premixed fuel equivalence ratio)	0.3	0.3

CHEMKIN program as well as the thermodynamic information for each cell. The CHEMKIN simulation provides information on the new species and energy release after solving the chemistry [32,33]. For the modeling of the diesel fuel oxidation, an internal chemical mechanism was used by AVL-FIRE software. In the present paper, three premixed fuel types (natural gas, methanol, and hydrogen) were ignited by pilot diesel fuel. The GRI-Mech 3.0 chemical kinetic mechanism, which consists of 53 species and 325 reactions, was used to describe the premixed natural gas oxidation [34] where the natural gas was represented by methane. The GRI-Mech 3.0 chemical kinetic mechanism accounts for the detailed oxidation reaction mechanism of hydrogen and thus the GRI-Mech 3.0 was used for premixed hydrogen oxidation as well. A reduced mechanism, which consists of 21 species and 93 reactions, was used for premixed methanol oxidation chemistry [35]. The extended Zeldovich mechanism was used for NO_x formation and Frolov kinetic soot model was used to predict the formation and oxidation of soot [36].

3.2. Model validation

The numerical model validation was achieved using the experimental data of three different premixed fuels, i.e. natural gas/diesel, hydrogen/diesel, and methanol/diesel. For natural gas/diesel dual-fuel combustion, the experimental data was obtained using Ricardo E6/MS engine. The specifications of the Ricardo engine for the present study are given in Table 2. For the purpose of this validation, two different engine operating conditions were selected. The CAD model of the combustion chamber geometry was generated using Catia software. The computational mesh of the Ricardo combustion chamber at the top dead center (TDC) is shown in Fig. 2. In order to reduce the computational time, and due to symmetry, only half of the geometry was used for the simulation. Due to the special shape of the combustion chamber, a large number of cells with a small size were allotted to the prechamber in order to provide good accuracy. In order to examine mesh independency, three computational grids with different average cell sizes of 0.4, 0.8, and 1.2 mm were generated. This resulted in 204,664, 135,448, and 91,428 cells at the bottom dead center (BDC) for each computational grid. An optimized average cell size of 0.8 mm, with less than 0.55% uncertainty was selected, which consisted of 135,448 cells at the BDC and 76,109 cells at the TDC. Further refinement of the computational mesh was found to insignificantly affect the model predictions. Moreover, a time step of 0.2 °CA was found to provide a good numerical accuracy and computation stability. The pre-combustion chamber and cylinder head mesh was kept stationary whereas that of the piston bowl was made from a moving mesh. Calculations were carried out for the closed portion of the cycle from the inlet valve closing (IVC) to the exhaust valve opening (EVO). The initial pressure was set by measuring the pressure at the IVC (Table 3) and the initial temperature at IVC was calculated using ideal gas law and using the inlet temperature after the heater (Table 3). All cells in the calculation domain were set to have a uniform initialization. The initial values of turbulence kinetic energy, turbulence length scale, turbulence dissipation rate, and swirl were set, respectively, as 25 m^2/s^2, 0.0045 m, 4654 m^2/s^3, and 2500 1/min [32]. The wall temperature was kept constant at 400 K. Fig. 3 shows a comparison of the in-cylinder pressure as predicted by the multi-dimensional CFD mechanism with the experimental data of the natural gas/diesel dual-fuel combustion. This figure shows that the cylinder pressure curves predicted by the present numerical simulation are in good agreement with the experimental results for the two cases in Table 3. It can be seen that, the peak pressure and its magnitude are well predicted by the present comprehensive CFD-chemistry model.

In order to strengthen the accuracy of the simulation, the numerical model was also validated by comparing the calculation with the experimental data of hydrogen/diesel and methanol/diesel dual-fuel cases at different operating conditions. Engines specifications along with the operating conditions are listed in Table 6. For the hydrogen/diesel dual-fuel simulation, hydrogen was introduced to the intake manifold and mixed with incoming air [20]. The intake pressure and temperature were kept constant at 200 kPa and 30 °C. The pilot diesel fuel was introduced at a rate of 3 mg/cycle. The injection started at 13 °BTDC and the injection duration of the pilot diesel fuel was set at 3.5 °CA. The comparison between calculation and experiment is shown in Fig. 4. This figure shows that the calculated in-cylinder pressure, heat release rate (HRR), and NO_x emissions are in good agreement with their experimental counterparts, indicating good reliability of the mechanisms and models used in the present numerical code to simulate dual-fuel combustion and performance.

The simulation of methanol/diesel dual-fuel combustion was also validated with the experimental data of Yoshida et al. [27]. Methanol was introduced to the intake manifold where methanol–air mixtures were drawn into the cylinder. The boost pressure was maintained at 101.3 kPa and the intake temperature was kept at room conditions. Diesel fuel was directly injected into the cylinder at 14 °BTDC. Fig. 5a and b presents a comparison of the in-cylinder pressure and NO_x emissions as predicted by multi-dimensional CFD model with their experimental counterparts. These figures show a reasonable agreement between the computed and measured in-cylinder pressure and NO_x emissions.

4. Results and discussions

The validated numerical model is used in this section to examine the effect of equivalence ratio of various premixed fuel types on

Table 4
Experimental uncertainty.

Parameter	Uncertainty (%)
Temperature	<2
Pressure	<2
Engine speed	<1
Fuel flow rate	<1
Air flow rate	<1

Table 5
Mathematical sub-models.

Turbulent model	RNG κ–ε
Break-up model	KH–RT
Evaporation model	Dukowicz
Wall heat transfer model	Standard wall function
Combustion model	CHEMKIN
Fuel chemistry	GRI-Mech 3.0 reduced methanol mech
Soot mechanism model	Frolov kinetic
NO_x mechanism model	Extended Zeldovich

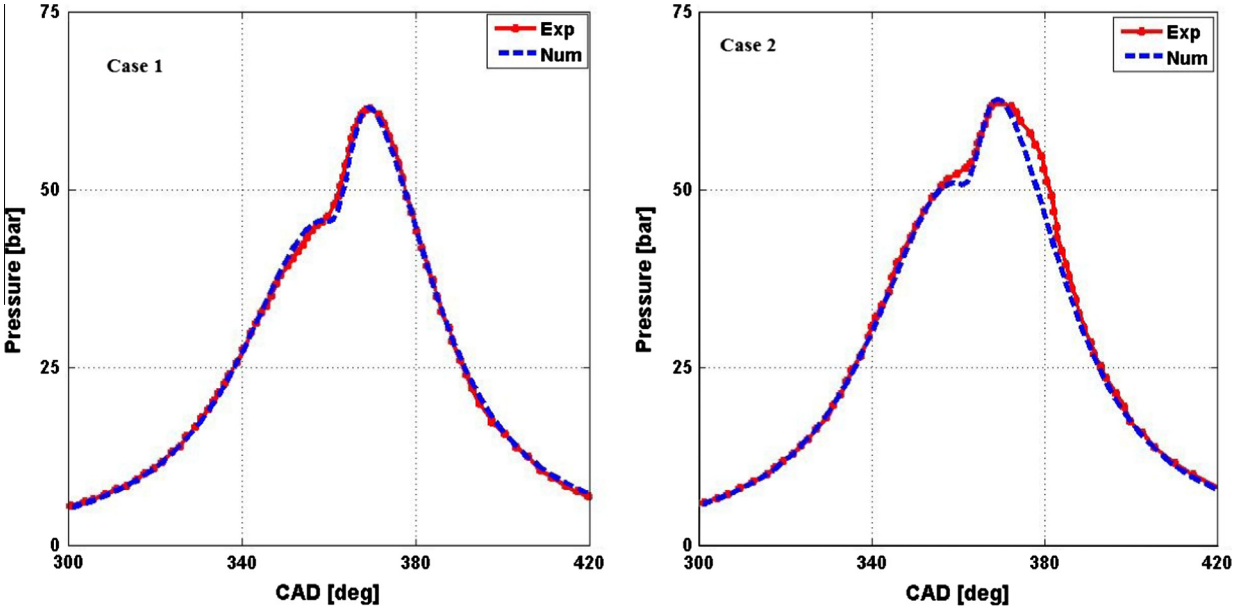

Fig. 3. Comparison of simulation and experimental results for natural gas/diesel Ricardo engine.

Table 6
Engine specifications and operating conditions.

Parameter/engine type	Hydrogen/diesel [20]	Methanol/diesel [27]
Bore (mm)	96	70
Stroke (mm)	108	55
Displacement (cc)	781.7	211
Compression ratio	16	19.9
Combustion chamber	Shallow-dish	Re-entrant
Injection type	DI	DI
Diesel fuel injection (mg/cycle)	3	2.8
Start of injection (°BTDC)	13	14
Nozzle hole × diameter (mm)	4 × 0.1	4 × 0.22
Engine speed (rpm)	1000	3000

dual-fuel pilot diesel ignition combustion. The engine used in the present paper is IDI Ricardo E6/MS dual-fuel engine and its specifications are listed in Table 2. The combustion chamber geometry and computational domain are mentioned in Section 3.2 and shown in Fig. 2. Case 2 of the operating/test conditions given in Table 3 is chosen as the base numerical conditions where a wide range of equivalence ratio (Φ_P = 0.15, 0.2, 0.25, 0.3, and 0.35) is examined for all premixed fuel types (i.e., natural gas/diesel, methanol/diesel, and hydrogen/diesel). Table 7 shows the mole fraction of the initial species for these considered fuels at the start of the numerical calculation.

4.1. Effect of premixed fuel type on combustion phasing

The average in-cylinder pressure (the average pressure throughout the main and pre-combustion chambers) and HRR at different equivalence ratios (Φ_P) are plotted in Fig. 6 for the three different premixed fuel types. A typical dual-fuel pilot ignition combustion process can be identified to take place in three stages. The first stage is a premixed combustion of the pilot diesel fuel and a small part of gaseous premixed fuel. The second stage is the premixed combustion of the gaseous fuel where the majority of gaseous fuel is burned which yields a significant rise in HRR. The third stage is the diffusion combustion of the residual pilot diesel fuel and gaseous premixed fuel [37]. Looking at Fig. 6, it can be clearly seen that, for all fuel mixtures, as the premixed fuel equivalence ratio rises, the peak in-cylinder pressure and HRR increase due to the higher fuel concentration inside the cylinder and overall richer operation. Moreover, increasing the premixed fuel equivalence ratio results advanced ignition timing. By comparing Fig. 6a–c, it is clear that hydrogen/diesel dual-fuel combustion has a steeper pressure rise rate and more advanced ignition timing. This is attributed to higher heating value and flame speed of hydrogen in comparison with natural gas and methanol fuels. The figure reveals also that the maximum combustion pressure (84.7 bar) and HRR (46.2 J/deg) occurred for hydrogen/diesel dual-fuel combustion with an equivalence ratio of 0.35. As shown in Fig. 6a, the position of peak pressure is retarded slightly when increasing the natural gas equivalence ratio while keeping the amount of pilot diesel fuel constant. Moreover, Fig. 6a shows that, the peak in-cylinder pressure increases by 23.8% when the equivalence ratio increases from 0.15 to 0.35. It can be seen in this figure that the HRR is not high enough at an equivalence ratio of 0.15 and consequently the mixture fails to burn completely. Hence the natural gas/diesel dual-fuel simulation case experiences partial burn at an equivalence ratio of 0.15. When observing the in-cylinder pressure and HRR in Fig. 6b, it can be remarked that at equivalence ratios of 0.15, 0.2, and 0.25, methanol/diesel dual-fuel combustion experiences misfiring phenomenon. This can be attributed to two factors. First, methanol has a high latent heat of vaporization. When using methanol as a premixed fuel, as part of its vaporization process, it absorbs heat from the fresh charge, lower its temperature. Second, methanol has a much lower ratio of specific heats compared to hydrogen and natural gas, which causes the temperature and pressure just before top dead center to be lower for the methanol case. The lower pressures and temperatures from these two effects lengthens ignition which excessively retards combustion phasing (Fig. 7b). On the other hand, as shown in Fig. 6c, hydrogen/diesel dual-fuel combustion with lean mixtures does not experience misfiring process. It can be seen that, increasing the hydrogen equivalence ratio slightly retards the peak pressure and HRR. However, in hydrogen/diesel case the combustion phasing is more advanced than that of both the natural gas/diesel and methanol/diesel dual-fuel simulation cases. HRR and in-cylinder pressure of hydrogen/diesel dual-fuel combustion tend to be higher than that of natural gas/diesel and methanol/diesel

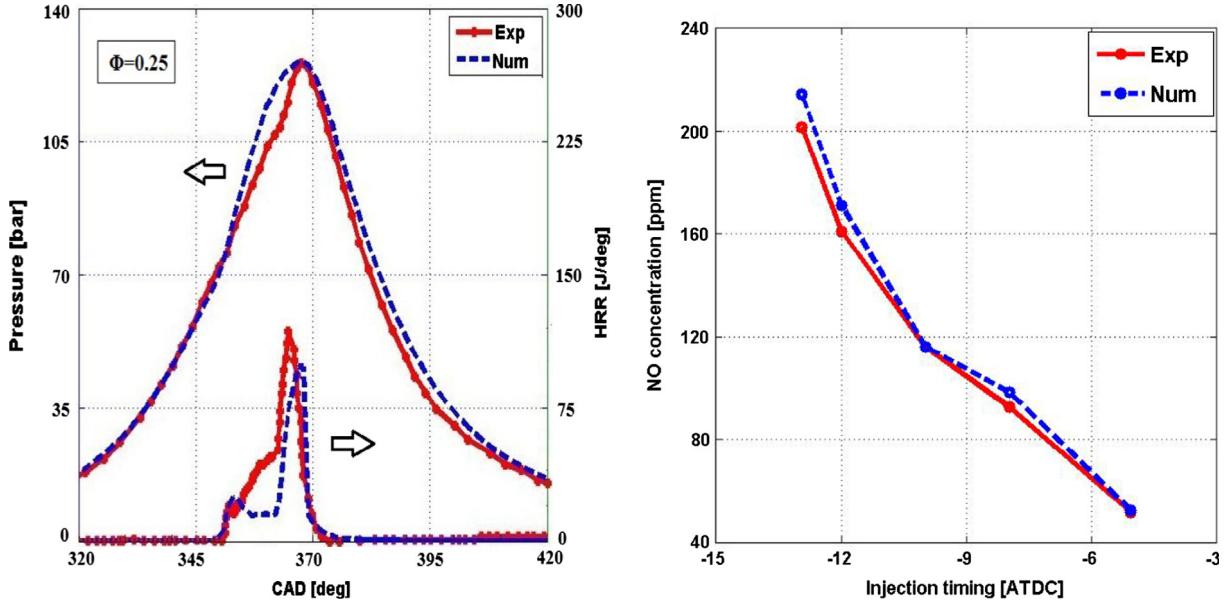

(a) In-cylinder pressure and HRR (b) NO_x emission

Fig. 4. In-cylinder pressure, HRR, and NO_x emissions of hydrogen/diesel dual-fuel engine.

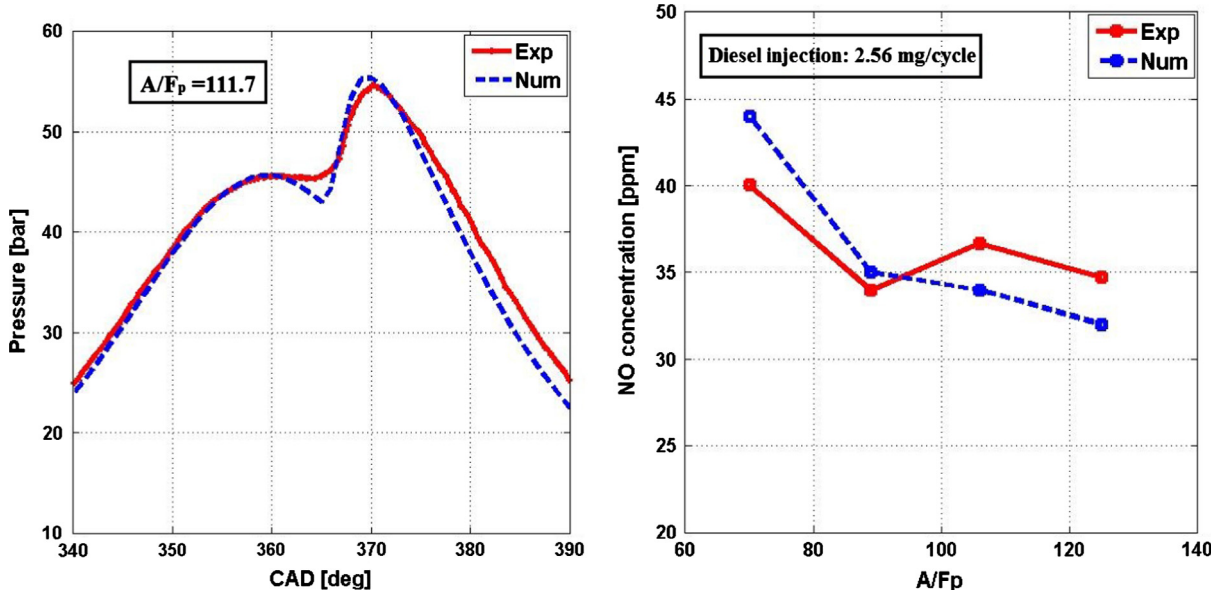

(a) In-cylinder pressure (b) NO_x emission

Fig. 5. In-cylinder pressure and NO_x emissions of methanol/diesel dual-fuel engine.

Table 7
Species mole fraction for the examined premixed fuels.

Φ_P	Species mole fraction (%)								
	Natural gas/diesel			Methanol/diesel			Hydrogen/diesel		
	CH_4	O_2	N_2	CH_3OH	O_2	N_2	H_2	O_2	N_2
0.15	0.0155	0.2068	0.7777	0.0205	0.2057	0.7738	0.0592	0.1976	0.7432
0.2	0.0205	0.2057	0.7738	0.0272	0.2043	0.7685	0.0775	0.1938	0.7287
0.25	0.0255	0.2047	0.7698	0.0338	0.2029	0.7633	0.095	0.1901	0.7149
0.3	0.0305	0.2036	0.7659	0.0403	0.2016	0.7581	0.1119	0.1865	0.7016
0.35	0.0354	0.2026	0.762	0.0467	0.2002	0.7531	0.1282	0.1831	0.6887

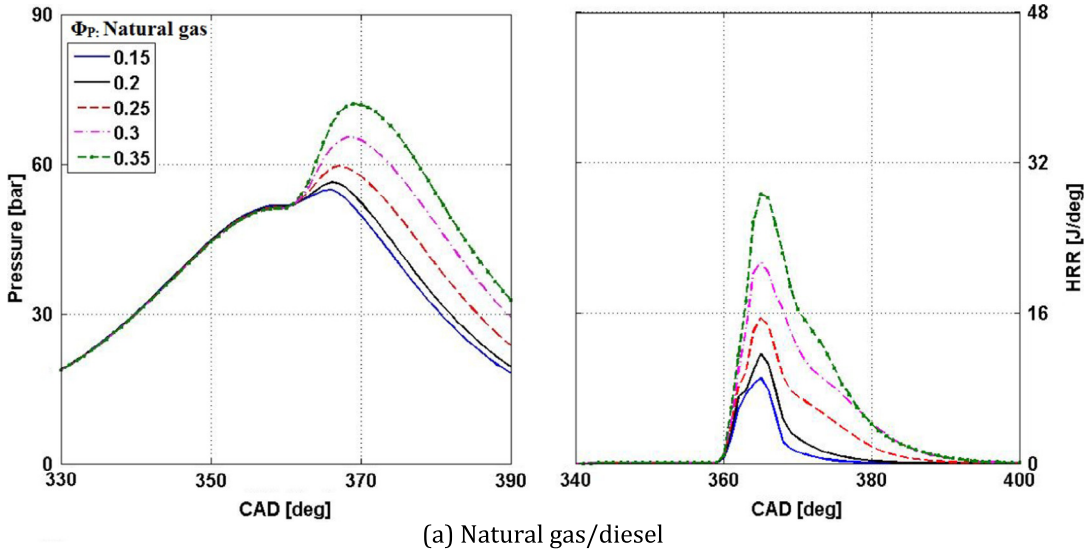

(a) Natural gas/diesel

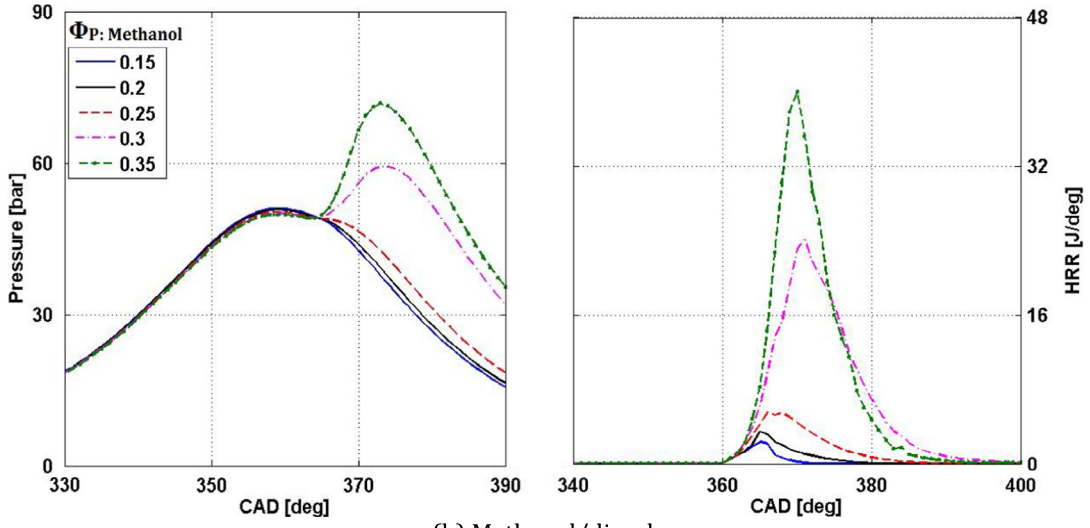

(b) Methanol/diesel

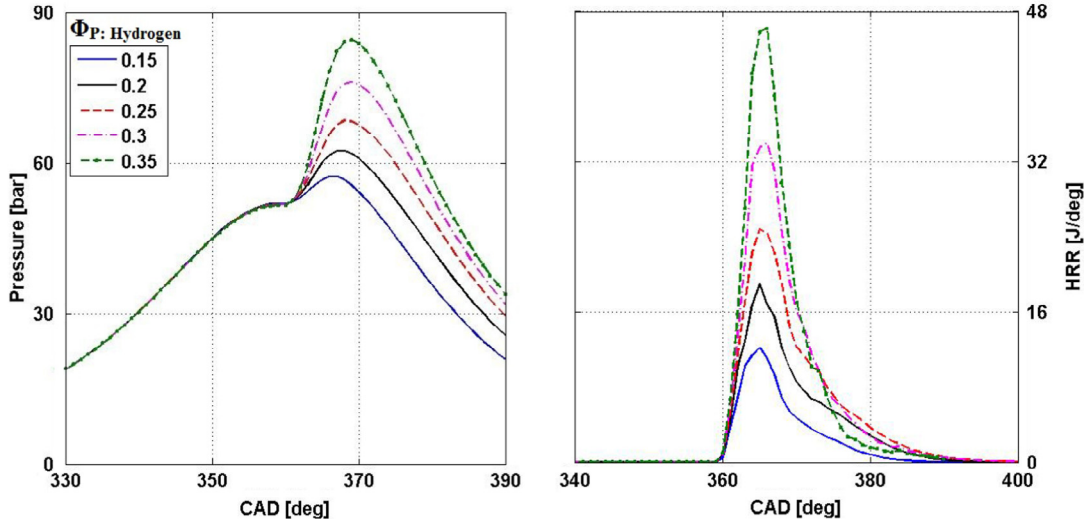

(c) Hydrogen/diesel

Fig. 6. In-cylinder pressure and HRR at different equivalence ratios for (a) natural gas/diesel, (b) methanol/diesel, and (c) hydrogen/diesel.

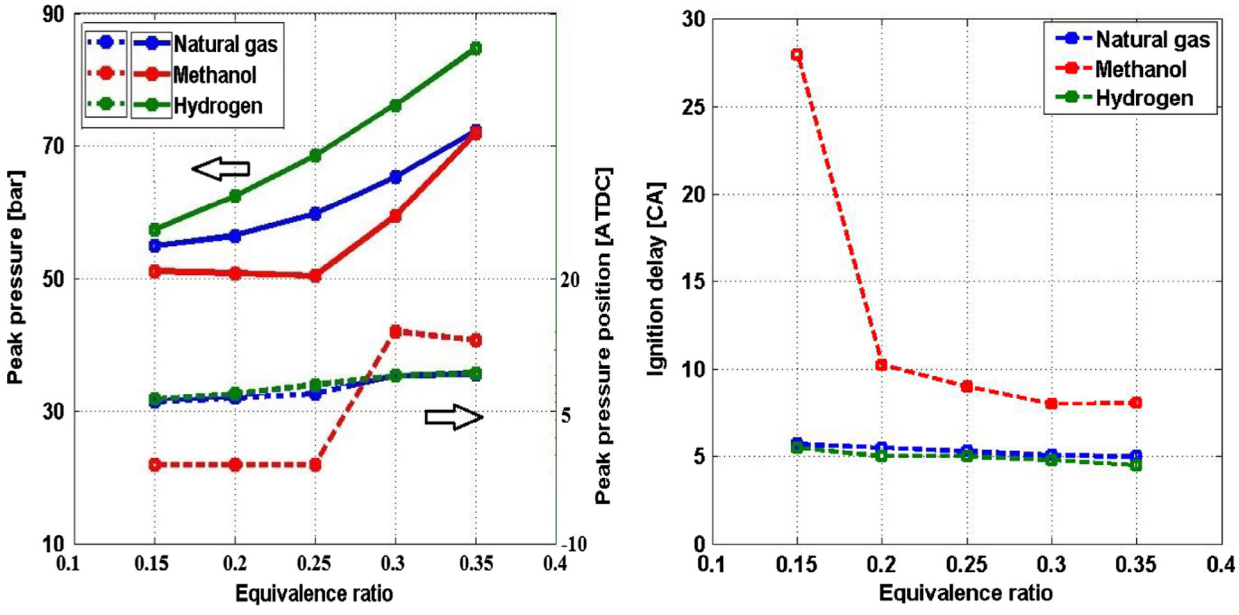

(a) In-cylinder peak pressure and its position (b) Ignition delay

Fig. 7. (a) In-cylinder peak pressure and its position, and (b) ignition delay for the three different premixed fuels.

dual-fuel engines which prevented misfiring phenomenon with very lean intake charge. The in-cylinder peak pressure increases by 32.2% when increasing the premixed equivalence ratio of hydrogen from 0.15 to 0.35.

Fig. 7a shows the effect of various premixed fuel types on the in-cylinder peak pressure and its position as a function of the equivalence ratio. It is clear that hydrogen/diesel dual-fuel simulation possesses the highest in-cylinder peak pressure. The peak pressure position is retarded slightly with increasing equivalence ratio for both natural gas and hydrogen. These results are in agreement with published findings for hydrogen/diesel case [20,38]. The figure shows that increasing the equivalence ratio of natural gas and hydrogen from 0.15 to 0.35 retards the locations of peak pressure by 3.1 and 2.9 °CA, respectively. In contrast, for equivalence ratios of 0.15, 0.2, and 0.25, the methanol/diesel simulation shows a relatively constant peak pressure at TDC due to the occurrence of misfiring phenomenon. However, the peak pressure increases considerably with an equivalence ratio ranging between 0.3 and 0.35.

Fig. 7b compares the effect of premixed fuels on the ignition delay in term of equivalence ratio. The ignition delay is defined as the duration, in CAD, between the start of injection (SOI = 2 °BTDC) and the start of combustion (SOC). In the present paper, SOC is defined by the crank angle at which 10% mass (pilot diesel and premixed fuels) fraction (CA_{10}) has burned [37]. It can be seen from Fig. 7b that increasing the premixed fuel equivalence ratio shortens the ignition delay. This trend is believed to be due to the elevated in-cylinder temperature arising from higher rates of low temperature fuel reaction kinetics which increases HRR and consequently advances the ignition timing. Both hydrogen/diesel and natural gas/diesel dual-fuel cases experience shorter ignition delay compared to methanol/diesel engine. As previously mentioned, methanol has a higher latent heat of vaporization and lower ratio of specific heats compared to hydrogen and natural gas. This results in a decrease in the temperature and pressure just before top dead center for the methanol case and consequently retards the combustion phasing which lengthens the ignition delay.

The in-cylinder temperature contours of natural gas/diesel, methanol/diesel, and hydrogen/diesel simulations are compared for five different engine crank angles at a constant premixed equivalence ratio (Φ_P) of 0.3 in Fig. 8. In order to understand the combustion process throughout the combustion chamber, the first cell layer which shows the constant wall temperature condition is removed and the temperature distribution of the inside cell layer is shown in Fig. 8. At −1 °ATDC, it can be seen that methanol/diesel dual-fuel engine has the lowest in-cylinder temperature at the end of the compression stroke, due to the high latent heat of vaporization of the fuel and the low ratio of specific heats. For methanol/diesel case there is no significant change in the temperature contours when further increasing the crank angle up to 3 °ATDC. After which, combustion is initiated due to the ignition of the pilot diesel fuel. This confirms the longer ignition delay of methanol/diesel dual-fuel case in comparison with natural gas/diesel and hydrogen/diesel cases (Fig. 7b). On the other hand, the temperature contours for both natural gas/diesel and hydrogen/diesel keep increasing in specific locations. High temperature cores can be seen at 1 °ATDC which is marked with black arrows. These cores are formed initially in the pre-combustion chamber where the pilot diesel fuel starts to oxidize. It should be noted that for all the examined fuels, the first indication of oxidation occurs in the pre-combustion chamber and then combustion expands to the main chamber. Combustion in methanol/diesel dual-fuel simulation starts at 3 °ATDC. Once combustion is underway, the hydrogen/diesel simulation shows the largest area of high-temperature (2000 K) regions, due to hydrogen's high heating value and high adiabatic flame temperatures. The lowest temperature in the cylinder during combustion occurs near the walls of the cylinder, chamber, and head and marked with blue arrows in Fig. 8.

Temporal concentration of mass fraction contours during the combustion process for the three premixed fuels at a constant equivalence ratio of 0.3 ($\Phi_P = 0.3$) are presented in Fig. 9. It can be seen that at 1 °ATDC, natural gas and hydrogen consumption is initiated at the regions where the diesel injection spray was targeted. After the oxidation of the diesel fuel at 3 and 5 °ATDC, there is a noticeable reduction in the natural gas and hydrogen. More rapid consumption rate of hydrogen leads to an increase in HRR and pressure which consequently narrow its HRR curve compared with that of natural gas (see Fig. 6a and c). In contrast,

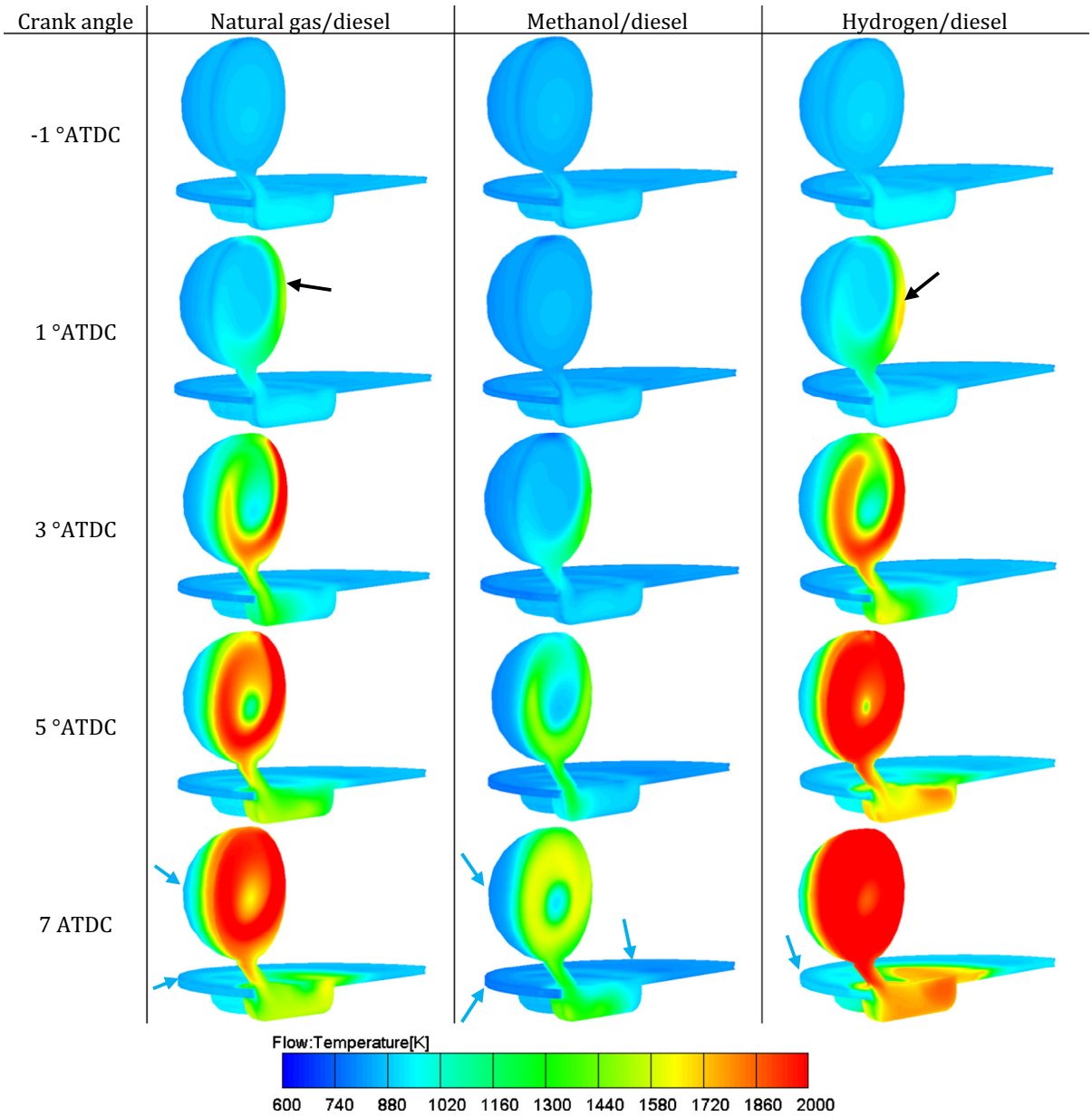

Fig. 8. Comparison of the in-cylinder temperature for three different premixed fuels at −1, 1, 3, 5 and 7 ATDC for $\Phi_P = 0.3$.

methanol starts to combust at 3 °ATDC where its consumption rate is very low which consequently results in a moderate pressure rise and HRR (see Fig. 6b).

4.2. Effect of premixed fuel type on engine performance

Fig. 10a presents the variation of the IMEP as a function of equivalence ratio for the different premixed fuels. The IMEP, which expresses the engine load, increased considerably with increasing the equivalence ratio for all premixed fuels. As shown in Fig. 6, the compression work decreases slightly and the expansion work increases considerably when increasing the equivalence ratio which results in a higher IMEP. Natural gas/diesel combustion undergoes the partial burn at an equivalence ratio of 0.15 which results in a negative IMEP. Also, methanol/diesel combustion shows a negative IMEP at equivalence ratios of 0.15, 0.2 and 0.25. In the leaner mixtures ($\Phi_P < 0.32$), hydrogen/diesel dual-fuel engine attains higher IMEP compared to that of natural gas/diesel and methanol diesel engines. However, methanol/diesel engine attains the highest IMEP at an equivalence ratio of 0.35. This is because at an equivalence ratio of 0.35, methanol/diesel engine experienced more retarded SOC (Fig. 6) which led to an increase in the expansion work considerably; however, compression work is lower than that of natural gas/diesel and hydrogen/diesel cases. Consequently, the total work and thus IMEP increased for methanol/diesel dual-fuel operation.

The variation of the ITE is shown in Fig. 10b where the partial burned and misfired cases are omitted and only the normal combustion cases are considered. ITE is calculated as the ratio of power output from the engine to the combined energy input from both premixed and direct fuels. As shown in this figure, the hydrogen/diesel case has the highest ITE in the leaner mixtures region which increases with increasing the hydrogen fuel. A parametric study of ITE for the hydrogen/diesel dual-fuel simulation case resulted in a minimum of 9.89% and a maximum of 56.24% when increasing the equivalence ratio from 0.15 to 0.35. At rich mixtures, methanol/diesel dual-fuel combustion has the highest ITE. The maximum ITE for the methanol/diesel dual-fuel simulations is

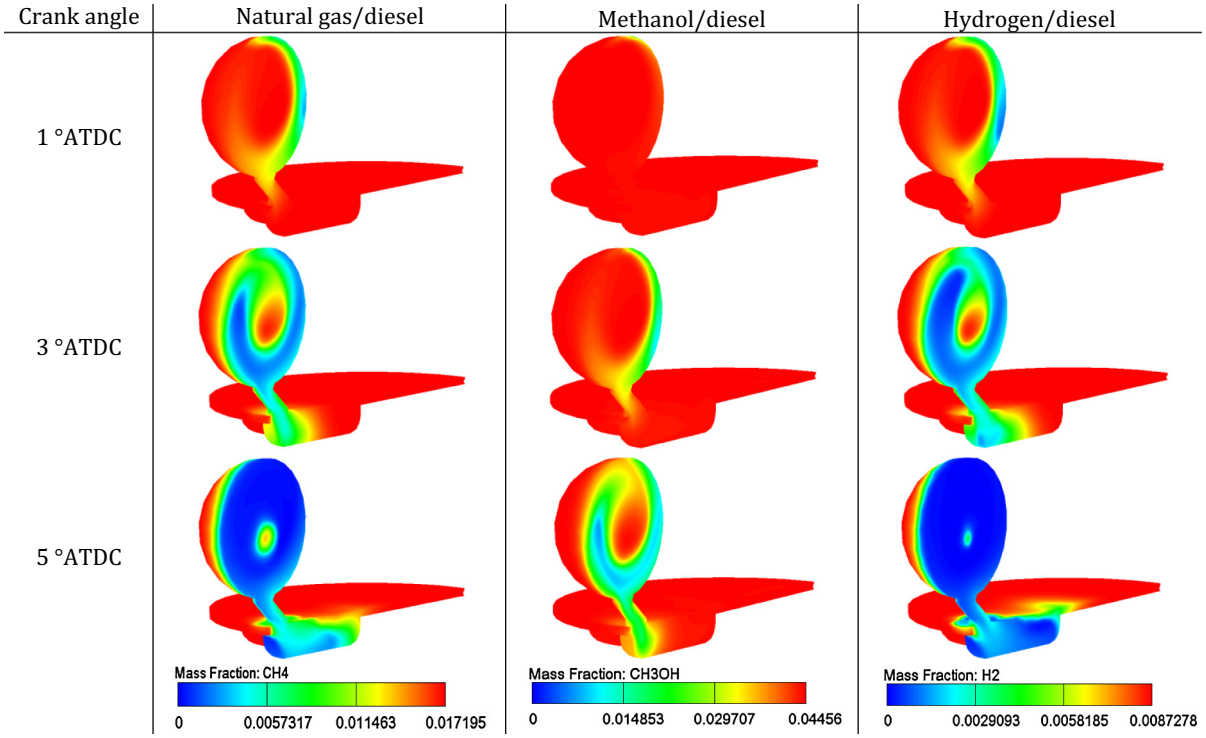

Fig. 9. Distribution of premixed fuels mass fraction at 1, 3 and 5 °ATDC for $\Phi_P = 0.3$.

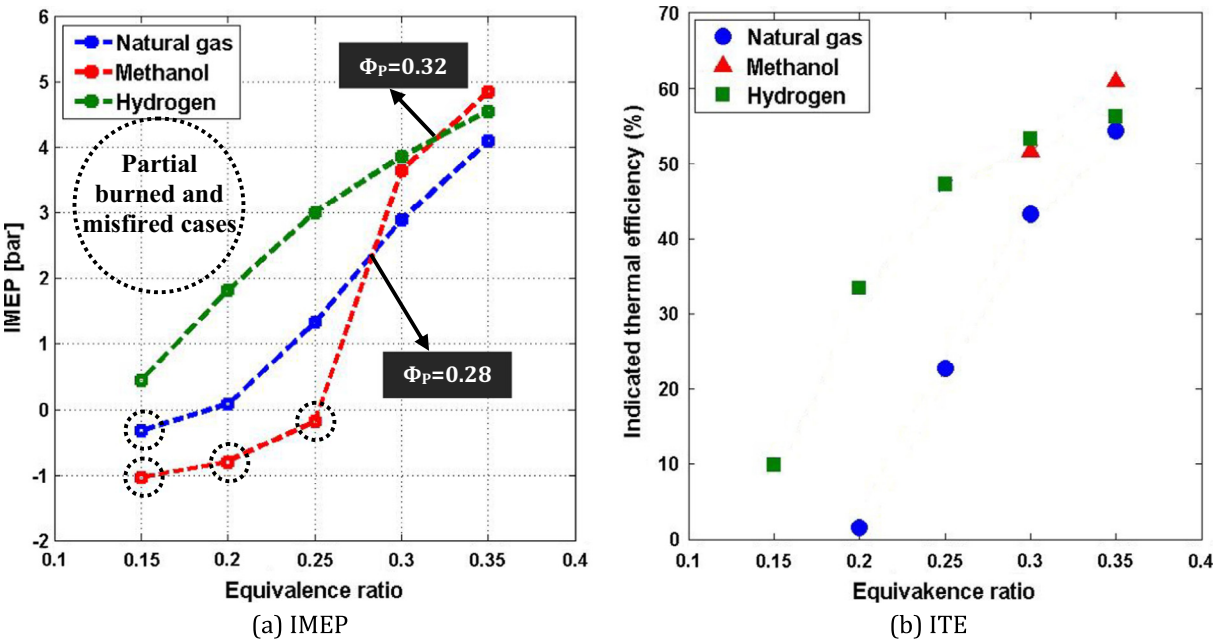

Fig. 10. Variation of IMEP and ITE with the equivalence ratio for the three different premixed fuels.

60.85% which occurs at an equivalence ratio of 0.35. Furthermore, the natural gas/diesel dual-fuel simulations exhibit the lowest ITE at all equivalence ratios. The maximum ITE for natural gas/diesel combustion is 54.31% which occurs at an equivalence ratio of 0.35 and the minimum ITE is 1.61% which occurs at an equivalence ratio of 0.2. The trends exhibited by the variation of IMEP and ITE in Fig. 10 are in good agreement with their experimental counterparts for natural gas/diesel mixture [14], methanol/diesel mixture [39], and hydrogen/diesel mixture [20,21,38].

4.3. Effect of premixed fuel type on emissions

4.3.1. NO_x emission

NO_x emissions in dual-fuel pilot ignition combustion are affected by three main factors: local gas temperature, oxygen concentration, and reaction duration [40]. Fig. 11a compares the NO_x mass fraction for various premixed fuels as a function of the equivalence ratio. As mentioned earlier, methanol as a premixed fuel results in lower in-cylinder temperatures (Fig. 8) and leading

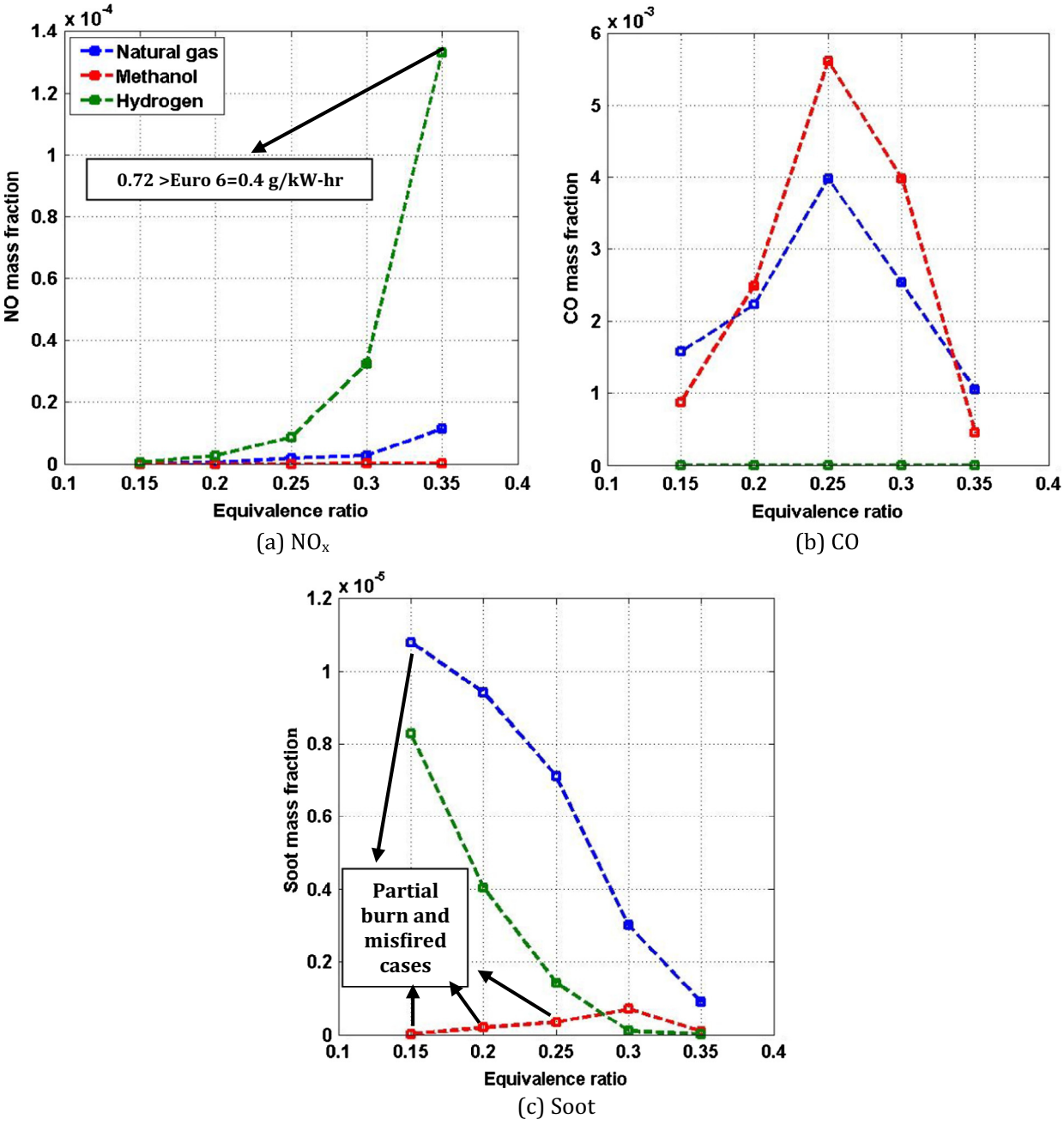

Fig. 11. Effect of premixed fuels on CO, NO_x, and soot emissions at EVO.

to poor combustion. Consequently, the NO_x mass fractions of the methanol/diesel case are much lower than that of natural gas/diesel and hydrogen/diesel cases. Due to its heating value, hydrogen/diesel combustion exhibits a significantly higher peak pressures and temperatures than those of natural gas/diesel and methanol/diesel cases (see Fig. 6). The higher temperatures yield a significant amount of NO_x emissions from the hydrogen/diesel dual-fuel simulation. Usually, the dual-fuel engine's flame temperatures is less than that of diesel engine as most of the fuel burns under lean premixed conditions. Hence, NO_x emissions of the dual-fuel engines tend to be lower than that of diesel engines [41]. In the present study hydrogen/diesel combustion generates the maximum of NO_x mass fraction which occurs at an equivalence ratio of 0.35. This NO_x when converted into g/kW h results in 0.72 g/kW h which exceeds the Euro 6 NO_x limits at 0.4 g/kW h [42]. To further gain insight into the mechanism of NO_x formation, contours of NO_x mass fraction for the three different premixed fuels at 10 and 20 °ATDC with an equivalence ratio of 0.3 is presented in Fig. 12. This figure shows that NO_x emissions of methanol/diesel dual-fuel combustion are much lower than that of hydrogen/diesel engine. In addition to heating value of methanol, its retarded ignition timing (see Fig. 6b) results in lower peak temperatures which consequently results in a reduction in NO_x emissions.

4.3.2. CO emission

Fig. 11b depicts the variation of CO mass fraction as a function of the equivalence ratio for the three different premixed fuels. It is observed that hydrogen/diesel combustion generates no CO

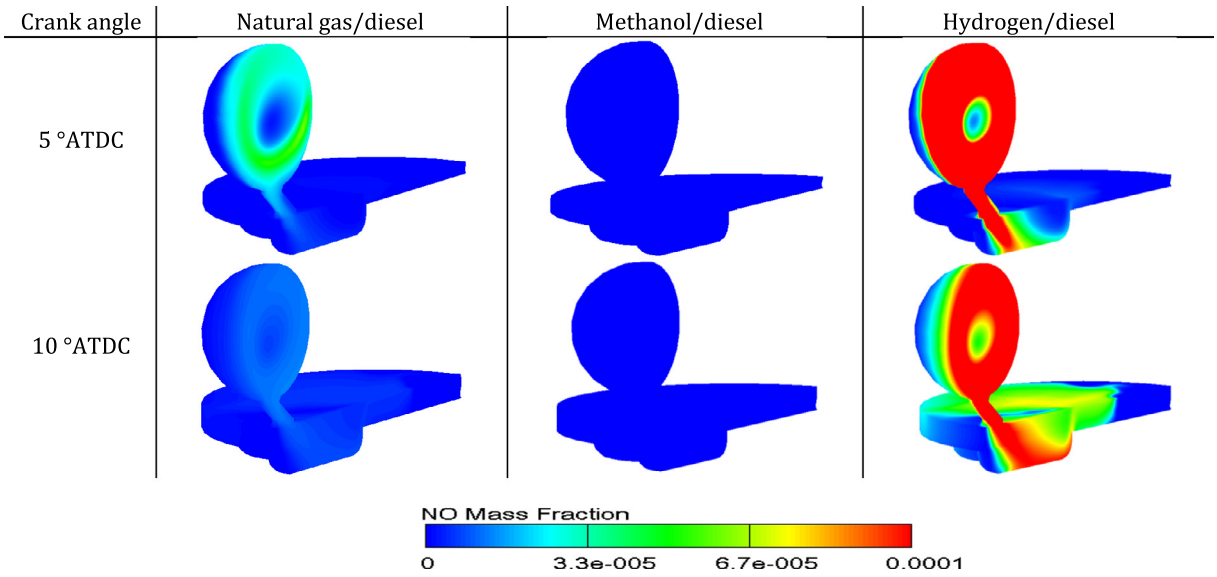

Fig. 12. Distribution of NO_x mass fraction of the three different premixed for 10 and 20 °ATDC fuels at $\Phi_P = 0.3$.

emissions because there is no carbon in the fuel. The only CO emissions could be formed from the diesel fuel, which oxidizes first and early and has plenty of time to complete oxidation to CO_2. On the other hand, natural gas/diesel and methanol/diesel dual-fuel cases generate higher amount of CO emissions where the maximum amount of CO emissions are produced with an equivalence ratio of 0.25. Leaner premixed mixtures ($\Phi_P < 0.25$) leading to poor combustion efficiency as well as CO oxidation, which gives rise to more CO emissions. As the premixed equivalence ratio of natural gas and methanol increases, the ignition timing advances and combustion temperature increases which promotes the oxidation of CO. Moreover, the oxygen content of methanol has positive impact on CO reduction [42]. It can be seen in this figure that, at an equivalence ratio of 0.35, methanol/diesel dual-fuel combustion produces lower CO emissions than that of natural gas/diesel. Temporal and spatial contours of CO mass fraction of the three premixed fuels at 5 and 10 °ATDC for an equivalence ratio of 0.3 are shown in Fig. 13. As shown in this figure, CO species is produced at the initial combustion stage. It is shown that more CO is produced for natural gas/diesel case at 5 °ATDC. However, CO is continuously oxidized during combustion, which results in lower CO emissions for natural gas/diesel at 10 °ATDC compared to methanol/diesel. Although methanol is an oxygenated fuel which promotes CO oxidation, the longer combustion duration of methanol/diesel combustion (see Fig. 6b) dominates, which yields an increase in CO emissions at an equivalence ratio of 0.3.

4.3.3. Soot emission

Fig. 11c shows the variation of soot emissions for the three premixed fuels. In normal combustion cases, soot emissions show an obvious drop with increased premixed fuel equivalence ratio. With more premixed fuel being introduced, dual-fuel pilot diesel ignition combustion can occur under more homogeneous conditions, thereby reducing soot emissions [43]. Hydrogen combustion produces only water and it does not form any soot emissions [44]. The lower soot emissions of hydrogen/diesel dual-fuel combustion compared to natural gas/diesel and methanol/diesel (except misfired cases) is caused by the absence of carbon in the premixed fuel. Fig. 14 presents the temporal and spatial contours of soot mass fraction of the three different premixed fuels at 5, 10,

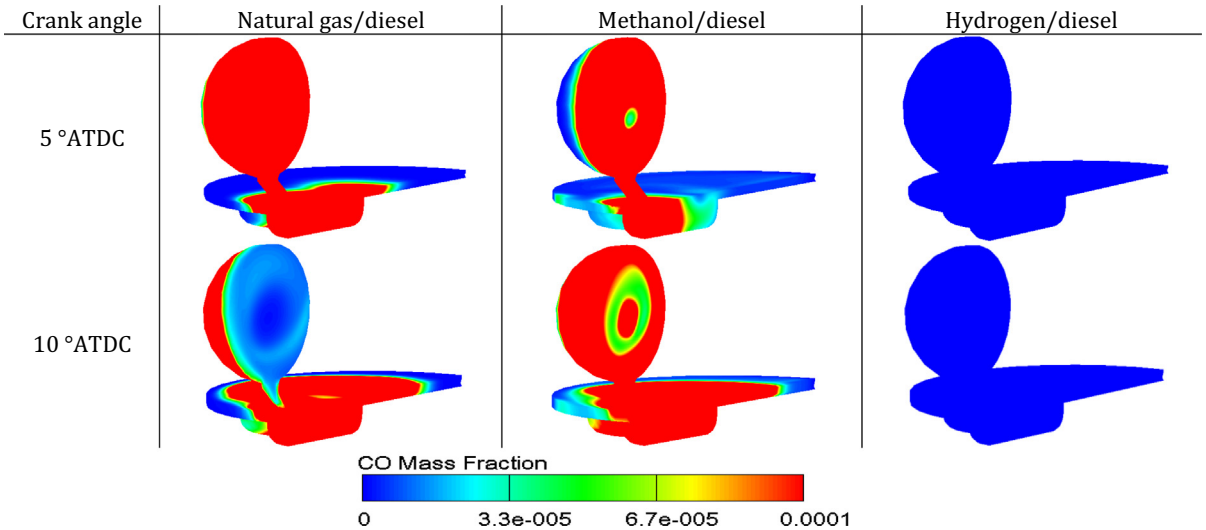

Fig. 13. Distribution of CO mass fraction for the three different premixed fuels at 10 and 20 °ATDC and $\Phi_P = 0.3$.

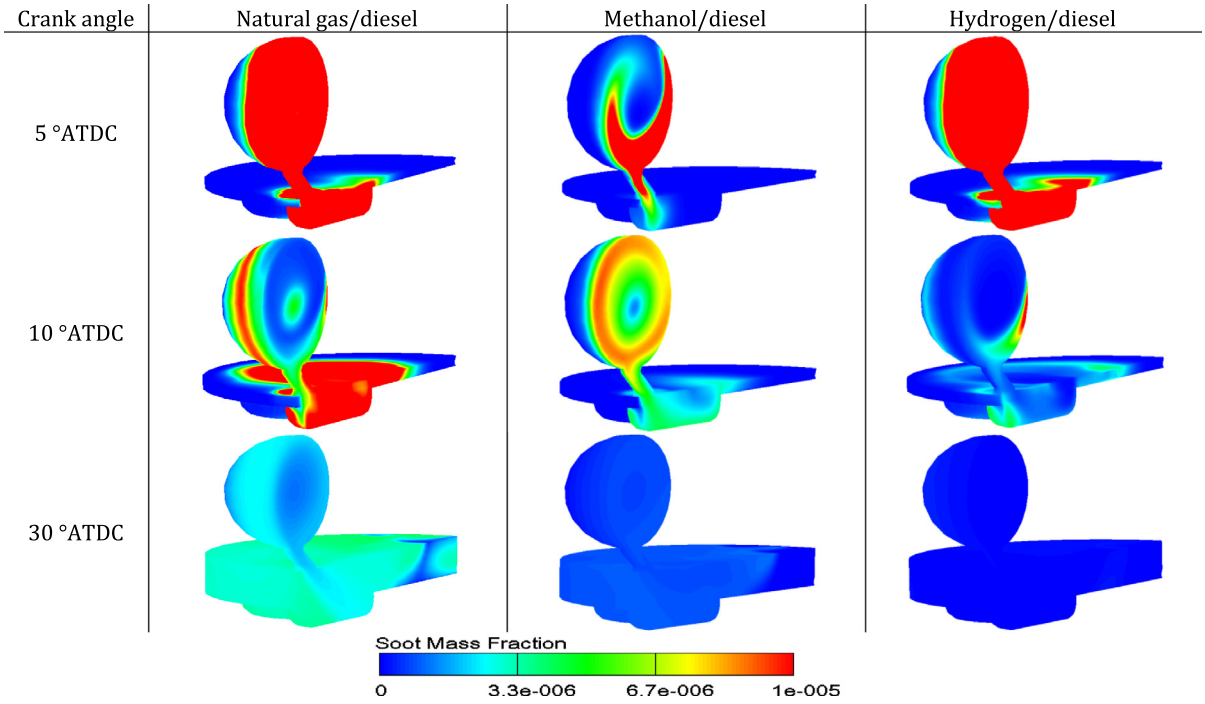

Fig. 14. Distribution of soot mass fraction for the three different premixed fuels at 5, 10 and 30 °ATDC and $\Phi_P = 0.3$.

30 °ATDC and an equivalence ratio of 0.3. As can be observed from this figure, during the first stage of the combustion (5 °ATDC), the hydrogen/diesel and natural gas/diesel simulations produce more soot emissions compared to methanol/diesel. However, soot oxidation is promoted for hydrogen/diesel case at a crank angle evolution (10 °ATDC) due to the higher gas temperatures and the final soot mass fraction is much lower than that of natural gas/diesel and methanol/diesel.

5. Conclusions

The effects of different premixed fuels (i.e., natural gas, methanol, and hydrogen) and their equivalence ratios (i.e., $\Phi_P = 0.15$, 0.2, 0.25, 0.3, and 0.35) on the combustion process, performance, and emissions of a dual-fuel IDI diesel engine were investigated. In addition to its validation, the present CFD modeling predictions showed good agreement with limited/available published data which is a further evidence of its reliability. The main findings are summarized as follows:

- At the same operating conditions, hydrogen/diesel dual-fuel combustion experiences steeper pressure rise rate and more advanced ignition timing. Increasing the equivalence ratio from 0.15 to 0.35, increases the in-cylinder peak pressure by 32.2% for hydrogen/diesel and 23.8% for natural gas/diesel while the location of peak pressure is retarded by 2.9 °CA and 3.1 °CA for hydrogen/diesel and natural gas/diesel engine, respectively. Natural gas/diesel dual-fuel combustion experiences partial burn at an equivalence ratio of 0.15, whereas methanol/diesel experiences misfiring at equivalence ratios of 0.15, 0.2 and 0.25. Moreover, methanol/diesel dual-fuel combustion exhibits a longer ignition delay compared to natural gas/diesel and hydrogen/diesel engines.
- Hydrogen induction as a premixed fuel enhances the diesel engine operation especially under leaner mixtures. At leaner mixture conditions ($\Phi_P < 0.32$), the hydrogen/diesel dual-fuel case has a higher IMEP compared to that of natural gas/diesel and methanol/diesel engines. However, under rich mixture conditions ($\Phi_P > 0.32$), the highest IMEP is achieved with methanol/diesel engine at an equivalence ratio of 0.35. Increasing the equivalence ratio increases the ITE for all three different premixed fuels. The maximum ITE (60.85%) is achieved with methanol/diesel dual-fuel combustion at an equivalence ratio of 0.35. ITE registered a minimum of 9.89% and a maximum of 56.24% at equivalence ratios of 0.15 and 0.35 for hydrogen/diesel engine. Natural gas/diesel dual-fuel engine shows the lowest ITE at all equivalence ratios. The maximum ITE is 54.31% at an equivalence ratio of 0.35 and its minimum is 1.61% at an equivalence ratio of 0.2 for natural gas/diesel dual-fuel engine.
- Methanol/diesel dual-fuel combustion has the lowest in-cylinder temperature which results in the lowest NO_x emissions. On the other hand, hydrogen enhances the diesel combustion and considerably increases the in-cylinder peak pressure and temperature. Therefore, hydrogen/diesel dual-fuel combustion generates the highest NO_x emissions at an equivalence ratio of 0.35, which exceeds the Euro 6 NO_x limitation. On the other hand, the hydrogen/diesel dual-fuel simulation experiences CO-free combustion. For both natural gas/diesel and methanol/diesel engines, the maximum CO emissions is generated at an equivalence ratio of 0.25. This is because further increasing the premixed equivalence ratio leads to an increased combustion temperature which in turn reduces the CO emissions. Natural gas/diesel and hydrogen/diesel simulations produce higher soot emissions under lean mixture conditions. Increasing the equivalence ratio decreases the soot emissions for all normal combustion cases. Hydrogen/diesel engine generates the lowest soot emission compared to both natural gas/diesel and methanol/diesel cases under rich mixture conditions.
- Overall, hydrogen/diesel combustion shows better combustion performance and efficiency and reduced emissions under leaner fuel mixture conditions. On the other hand, methanol/diesel dual-fuel combustion performs better in terms of engine performance and emissions reduction under rich mixture conditions.

References

[1] Geng Peng, Yao Chunde, Wei Lijiang, Liu Junheng, Wang Quangang, Pan Wang, et al. Reduction of PM emissions from a heavy-duty diesel engine with diesel/methanol dual-fuel. Fuel 2010;89:1397–406.

[2] Liu Jie, Yang Fuyuan, Wang Hewu, Ouyang Minggao, Hao Shougang. Effects of pilot fuel quantity on the emissions characteristics of a CNG/diesel dual-fuel engine with optimized pilot injection timing. Appl Energy 2013;110:201–6.

[3] Maurya Rakesh Kumar, Agarwal Avinash Kumar. Experimental study of combustion and emission characteristics of ethanol fuelled port injected homogeneous charge compression ignition (HCCI) combustion engine. Appl Energy 2011;88:1169–80.

[4] Bedoya Ivan D, Saxena Samveg, Cadavid Francisco J, Dibble Robert W, Wissink Martin. Experimental study of biogas combustion in an HCCI engine for power generation with high indicated efficiency and ultra-low NOx emissions. Energy Convers Manage 2012;53:154–62.

[5] Sudheesh K, Mallikarjuna JM. Diethyl ether as an ignition improver for biogas homogeneous charge compression ignition (HCCI) operation – an experimental investigation. Energy 2010;35:3614–22.

[6] Abdelaal MM, Hegab AH. Combustion and emission characteristics of a natural gas-fueled diesel engine with EGR. Energy Convers Manage 2012;64:301–12.

[7] Yang Zhenzhong, Chu Chaoyang, Wang Lijun, Huang Yan. Effects of H_2 addition on combustion and exhaust emissions in a diesel engine. Fuel 2015;139:190–7.

[8] Shi, Yu, Ge, Hai-Wen, Reitz, Rolf D. Computational optimization of internal combustion engines. London, Dordrecht, Heidelberg, New York: Springer. http://dx.doi.org/10.1007/978-0-85729-619-1.

[9] Yap D, Peucheret SM, Megaritis A, Wyszynski ML, Xu H. Natural gas HCCI engine operation with exhaust gas fuel reforming. Int J Hydrogen Energy 2006;31:587–95.

[10] Zheng Junnian, Caton Jerald A. Effects of operating parameters on nitrogen oxides emissions for a natural gas fueled homogeneous charged compression ignition engine (HCCI): results from a thermodynamic model with detailed chemistry. Appl Energy 2012;92:386–94.

[11] Santoso WB, Bakar RA, Nur A. Combustion characteristics of diesel–hydrogen dual-fuel engine at low load. Energy Proc 2013;32:3–10.

[12] Sayin Cenk, Ilhan Murat, Canakci Mustafa, Gumus Metin. Effect of injection timing on the exhaust emissions of a diesel engine using diesel–methanol blends. Renewable Energy 2009;34:1261–9.

[13] Zhou JH, Cheung CS, Leung CW. Combustion, performance and emissions of a diesel engine with H_2, CH_4 and H_2–CH_4 addition. Int J Hydrogen Energy 2014;39:4611–21.

[14] Imran S, Emberson DR, Diez A, Wene DS, Crookes RJ, Korakianitis T. Natural gas fueled compression ignition engine performance and emissions maps with diesel and RME pilot fuels. Appl Energy 2014;124:354–65.

[15] Kong Song-Charng. A study of natural gas/DME combustion in HCCI engines using CFD with detailed chemical kinetics. Fuel 2007;86:1483–9.

[16] Agarwal AK. Biofuels (alcohols and biodiesel) applications as fuels for internal combustion engines. Prog Energy Combust Sci 2007;33:233–71.

[17] Zhang ZH, Cheung CS, Yao CD. Influence of fumigation methanol on the combustion and particulate emissions of a diesel engine. Fuel 2013;111:442–8.

[18] Li Yaopeng, Jia Ming, Liu Yaodong, Xie Maozhao. Numerical study on the combustion and emission characteristics of a methanol/diesel reactivity controlled compression ignition (RCCI) engine. Appl Energy 2013;106:184–97.

[19] Zhou JH, Cheung CS, Leung CW. Combustion, performance, regulated and unregulated emissions of a diesel engine with hydrogen addition. Appl Energy 2014;126:1–12.

[20] Roy Murari Mohon, Tomita Eiji, Kawahara Nobuyuki, Harada Yuji, Sakane Atsushi. An experimental investigation on engine performance and emissions of a supercharged H_2-diesel dual-fuel engine. Int J Hydrogen Energy 2010;35:844–53.

[21] Talibi Midhat, Hellier Paul, Balachandran Ramanarayanan, Ladommatos Nicos. Effect of hydrogen–diesel fuel co-combustion on exhaust emissions with verification using an in-cylinder gas sampling technique. Int J Hydrogen Energy 2014;39:15088–102.

[22] Lounici Mohand Said, Loubar Khaled, Tarabet Lyes, Balistrou Mourad, Niculescu Dan-Catalin, Tazerout Mohand. Towards improvement of natural gas–diesel dual-fuel mode: an experimental investigation on performance and exhaust emissions. Energy 2014;64:200–11.

[23] Song Ruizhi, Liu Jie, Wang Lijun, Liu Shenghua. Performance and emissions of a diesel engine fuelled with methanol. Energy Fuels 2008;22:3883–8.

[24] Zhang ZH, Cheung CS, Chan TL, Yao CD. Experimental investigation of regulated and unregulated emissions from a diesel engine fueled with Euro V diesel fuel and fumigation methanol. Atmos Environ 2010;44:1054–61.

[25] Sandalci Tarkan, Karaggoz Yasin. Experimental investigation of the combustion characteristics, emissions and performance of hydrogen port fuel injection in a diesel engine. Int J Hydrogen Energy 2014;39:18480–9.

[26] Yousefi Amin, Gharehghani Ayatallah, Birouk Madjid. Comparison study on combustion characteristics and emissions of a homogeneous charge compression ignition (HCCI) engine with and without pre-combustion chamber. Energy Convers Manage 2015;100:232–41.

[27] Yoshida K, Shoji H, Tanaka H. Engine performance of lean methanol–air mixture ignited by diesel fuel injection applied with internal EGR. SAE paper 2000-01-2012; 2000.

[28] Han Z, Reitz RD. Turbulence modeling of internal combustion engines using RNG k–ε models. Combust Sci Technol 1995;106:267–95.

[29] Beale C, Reitz RD. Modelling spray atomization with the Kelvine Helmholtz/Rayleighe Taylor hybrid model. Atom Sprays 1999;9:623–50.

[30] Abagnale C, Cameretti MC, De Simio L, Gambino M, Iannaccone S, Tuccillo R. Numerical simulation and experimental test of dual-fuel operated diesel engines. Appl Therm Eng 2014;65:403–17.

[31] Dukowicz JK. Quasi-steady droplet change in the presence of convection. Informal report. Los Alamos Scientific Laboratory. LA7997-MS.

[32] AVL FIRE User Guide, Version 2011, AVL List Gmbh; 2009.

[33] Kee RJ, Rupley FM, Meeks E, Miller JA. Chemkin-iii: a Fortran chemical kinetics package for the analysis of gas-phase chemical and plasma kinetics. SAND96-8216. Sandia National Laboratory Technical, Report; 1996.

[34] Smith GP, Golden DM, Frenklach M, Moriarty NW, Eiteneer B, Goldenberg M, et al. GRI-mech3.0 data; 2006. <http://www.me.berkeley.edu/gri_mech.html>.

[35] Li J, Zhao Z, Kazakov A, Chaos M, Dryer FL, Scire Jr JJ. A comprehensive kinetic mechanism for CO, CH_2O, CH_3OH combustion. Int J Chem Kinet 2007;39:109–36.

[36] Evlampiev AV, Frolov SM, Basevich VYa, Belyaev AA. Chemical. Phys Rep 2001;20(1):21–7.

[37] Yang Bo, Xi Chengxun, Wei Xing, Zeng Ke, Lai Ming-Chia. Parametric investigation of natural gas port injection and diesel pilot injection on the combustion and emissions of a turbocharged common rail dual-fuel engine at low load. Appl Energy 2015;143:130–7.

[38] Liew C, Li H, Nuszkowski J, Liu S, Gatts T, Atkinson R, et al. An experimental investigation of the combustion process of a heavy-duty diesel engine enriched with H_2. Int J Hydrogen Energy 2010;35:11357–65.

[39] Liu Jie, Li Yi, Li Guangle, Zhu Zan, He Hun, Liu Shenghua. Effect of pilot diesel quantity and fuel delivery advance angle on the performance and emission characteristics of a methanol-fueled diesel engine. Energy Fuels 2010;24:1611–6.

[40] Kose H, Ciniviz M. An experimental investigation of effect on diesel engine performance and exhaust emissions of addition at dual-fuel mode of hydrogen. Fuel Process Technol 2013;114:26–34.

[41] Liu Jie, Yang Fuyuan, Wang Hewu, Ouyang Minggao. Numerical study of hydrogen addition to DME/CH_4 dual-fuel RCCI engine. Int J Hydrogen Energy 2012;37:8688–97.

[42] Commission regulation (EU) no 582/2011 (Euro VI), date is for new registrations. Off J Eur Union; 2011.

[43] Zhou DZ, Yang WM, An H, Li J, Shu C. A numerical study on RCCI engine fueled by biodiesel/methanol. Energy Convers Manage 2015;89:798–807.

[44] Bose PK, Maji D. An experimental investigation on engine performance and emissions of a single cylinder diesel engine using hydrogen as inducted fuel and diesel as injected fuel with exhaust gas recirculation. Int J Hydrogen Energy 2009;34:4847–54.